CTRC Research Publications   Cooling Technologies Research Center

2-3-2005

Infrared Micro-Particle Image Velocimetry Measurement in Silicon-Based Microdevices

Dong Liu

S V. Garimella
Purdue University, sureshg@purdue.edu

Steve Wereley
swereley@purdue.edu

Follow this and additional works at: http://docs.lib.purdue.edu/coolingpubs

Infrared Micro-Particle Image Velocimetry in Silicon-Based Microdevices

DONG LIU, SURESH V. GARIMELLA[§], AND STEVEN T. WERELEY

Cooling Technologies Research Center

School of Mechanical Engineering

Purdue University

West Lafayette, Indiana 47907-2088 USA

[§] Correspondence to: sureshg@ecn.purdue.edu

Abstract

A non-intrusive diagnostic technique, infrared micro-particle image velocimetry (IR-PIV), is developed for measuring flow fields within MEMS devices with micron-scale resolution. This technique capitalizes on the transparency of silicon in the infrared region, and overcomes the limitation posed by the lack of optical access with visible light to sub-surface flow in silicon-based micro-structures. Experiments with laminar flow of water in a circular micro-capillary tube of hydraulic diameter 255 µm demonstrate the efficacy of this technique. The experimental measurements agree very well with velocity profiles predicted from laminar theory. Cross-correlation and auto-correlation algorithms are employed to measure very-low and moderate-to-high velocities, respectively; the former approach is suitable for biomedical applications while the latter would be needed for measurements in electronics cooling. The results indicate that the IR-PIV technique effectively extends the application of regular micro-PIV techniques, and has great potential for flow measurements in silicon-based microdevices.

Nomenclature

d_e effective diameter of tracer particles on image plane

d_p diameter of tracer particles

D_h diameter of micro-capillary tube

e spacing between pixels of image detector

I intensity of recorded image

L_{fd} hydrodynamic entry length

M total magnification of microscope system

n refractive index

NA numerical aperture of objective lens

r radial position

r_0 radius of micro-capillary tube

r_{nom} nominal radius of micro-capillary tube

Δr radial misalignment

Re Reynolds number

t time

δt time interval between laser pulses

u axial velocity

u_m mean velocity

U velocity of fluid

δx measurement uncertainty

δz depth of field

δz_m measurement depth

Greek Symbols

λ wavelength of illumination light

μ_f fluid viscosity

θ angular misalignment

ρ density

τ relaxation time

1

Introduction

Over the past two decades, advances in microfabrication techniques have enabled the rapid development of micro-electro-mechanical systems (MEMS). MEMS devices are usually silicon-based functional microstructures that have feature sizes of order 1 to 100 µm. These small length scales have posed challenges for the measurement of flow and temperature fields with conventional techniques (Garimella and Sobhan 2002; Liu and Garimella, 2004). The difficulties are especially pronounced for microfluidic systems, where accurate determination of velocity, shear stress, temperature and heat flux is desired with micron-scale spatial resolution. Micro-particle image velocimetry (µ-PIV) is particularly suited for this purpose, if optical access to the flow can be provided.

Particle image velocimetry is a well-established non-intrusive technique for measuring flow fields, in which positions of tracer particles are recorded at two consecutive, known times and the displacements of the particles are analyzed statistically by correlating the particle images (Meinhart et al. 1993). To adapt this technique to microscale flows, Santiago et al. (1998) conducted micro-PIV experiments in a Hele-Shaw flow around a 30 µm major-diameter elliptical cylinder. The measurements had a spatial resolution of 6.9 µm × 6.9 µm × 1.5 µm, and were obtained using fluorescently tagged polystyrene particles of 300 nm diameter illuminated with a continuous Hg-arc lamp, and imaged by an EFT intensified CCD camera. In follow-on work, Meinhart et al. (1999) presented an alternative measurement approach with spatial resolution of 13.6 µm × 0.9 µm × 1.8 µm and velocity-vector spacing of 450 nm. A double-pulsed Nd:YAG laser of 532 nm wavelength was used to image smaller particles of 200 nm diameter in a 30 µm × 300 µm rectangular glass microchannel. The measured velocity field agreed to within 2% with analytical predictions.

As a diagnostic technique, micro-PIV requires optical access to the flow under investigation. If the substrate is not transparent, special optical windows have to be accommodated into the microfluidic devices. Such a requirement can seriously limit the use of this technique. Alternative approaches have been proposed to study flow in microdevices. Wu et al. (1995) reported NMR imaging of electrokinetic flow in larger tubes of 3 mm inner diameter. This technique was capable of providing 3D images of the flow with spatial resolution on the order of 10 µm. Lanzilloto et al. (1996) employed X-ray imaging to measure the flow field in a microchannel of 640 µm diameter by using oil-water emulsion droplets as tracers. The spacing of the velocity vectors acquired was roughly 40 µm, and axial bulk velocities of 7 to 14 µm/s could be measured. Although these techniques are able to yield sub-surface velocity measurements without optical access, they do not lend themselves easily to micron-scale resolution, and are costly to implement.

The relative transparency of silicon (transmittance of 50% in the near-infrared waveband, 1.0 µm to 2.2 µm) suggests that measurements can be made through silicon using an infrared illumination source for the study of microdevices, without the need for optical windows. An infrared thermal velocimetry system which exploited this IR-transparency of silicon was reported by Chung et al. (2003). An infrared laser pulse (wavelength 10.6 µm) was used to heat fluid in a silicon device, and the average velocity was deduced from consecutive infrared images of emitted radiation from the fluid transmitted through the silicon substrate. This approach is limited to the deduction of average flow rate (and not the velocity distribution), and

also has poor spatial resolution. Experiments by Breuer et al. (2001) adapted the micro-PIV technique to explore the flow field inside a silicon micro-nozzle with a throat width of 40 μm and depth of 300 μm. The motion of a solid rotor inside a microturbine was also measured using the time-of-flight technique. The velocity-vector fields obtained provided a preliminary demonstration for the applicability of this non-intrusive measurement technique. However, no quantitative comparisons were reported to validate the measured velocities against benchmark data or theoretical predictions.

A variety of important issues remain to be fully addressed in the development of infrared micro-PIV (IR-μPIV) as a diagnostic tool for velocity-field measurements. These include approaches for illumination, choice of tracer particle, timing sequence, imaging technique and the micro-PIV analysis algorithm. The present work provides a detailed discussion of these issues involved in the development of an IR-PIV system for measuring velocity distributions within MEMS devices with micron-scale resolution.

2

Experimental instrumentation

The experimental apparatus is schematically depicted in Fig. 1. It consists of a liquid delivery system (outlined on the left), the laser system and fiber optics (bottom center), the imaging system (top right) and the microchannel test piece. For very low-speed flows (~ 100 μm/s), the seeded water is pumped through the channel at a constant velocity using a micro-translation stage. For moderate-to-high speed flows (~ 1 m/s), the tracer particle-water mixture is driven by compressed nitrogen gas through the microchannel piece, and collected in a syringe. The pressure at the inlet of the microchannel is measured, and the collected fluid is accurately weighed to determine the mean flow velocity. Illumination is provided by a twin Nd:YAG laser system for moderate-to-high speed flows, and the laser beams are directed into the test piece using IR fiber optics so that the incident angle may be optimized by trial and error. For very low-speed flows, a high-intensity illuminator is employed as the light source. The tracer particle images are captured with a near-infrared (NIR) camera and then transferred to a computer for processing. Major components in Fig. 1 are discussed further in the following.

2.1

Laser System

The TWIN OPO system (OPOTEK, Inc.) consists of two main subsystems: twin lasers and an optical parametric oscillator (OPO). The two Nd:YAG lasers are triggered externally to generate collinear beam pulses of 4.9 ns at 1064 nm. The laser beams are then frequency-doubled to 532 nm before pumping the OPO. The OPO is a passive, nonlinear optical device which converts the pumping laser beam (532 nm) into signal and idler beams, tunable from 680 nm to 2400 nm. This wide waveband offers great flexibility in choosing the proper wavelength to optimize system performance.

2.2

Imaging System

A near-infrared camera (Alpha NIR from Indigo Systems) is employed for image capture. The sensor head of the NIR camera employs a 320×256 Indium Gallium Arsenide focal plane array (FPA) with pixel size of 30 μm, and is highly sensitive to energy in the 900 nm to 1700 nm wavelength range. A Mitutoyo infinity-corrected NIR microscope objective of 20 x, 0.4 numerical aperture (NA) is used in the experiment, offering a resolution of 0.7 μm. This imaging system has a field of view of 480 μm × 384 μm.

To determine the actual displacement of tracer particles in the flow field, the image-to-object ratio of the imaging system must be known *a priori*. The camera is calibrated for this purpose using 1951 USAF test patterns (Edmund Scientific), yielding a resulting scale of 1.481 µm/pixel; one pixel in the image plane is thus equivalent to 1.481 µm of physical displacement in the flow field.

2.3

Test Section

In order to validate the measured velocities against established theoretical predictions, the tests were conducted in a fused-silica micro-capillary tube (Polymicro, Inc.) of circular cross section with a 255 µm diameter. The total tube length is 12.04 cm. The transmittance curves for fused silica and silicon (www.Thermo.com, 2004) are shown in Fig. 2. Since silicon microdevices are the target application in this work, a standard 2-inch silicon wafer of 500 µm thickness was placed between the micro-capillary tube and the incident laser beam in the experiments to simulate transmission through a silicon substrate.

2.4

Tracer Particles

In conventional micro-PIV experiments, inelastic scattering techniques, such as epi-fluorescence, are often used to image sub-micron particles (Meinhart et al., 1999). However, fluorescent dyes with both excitation and emission wavelengths in the infrared waveband are unavailable. Hence, elastic scattering techniques are needed in IR-PIV measurements. The size of the tracer particle is chosen from a trade-off between adequate tracking capability requiring small particles, and sufficient light-scattering which requires large particles (Melling, 1997).

Tracking characteristics of tracer particles can be expressed in terms of the relative velocity lag (Raffel et al., 1998), which reflects the extent to which particles faithfully follow the motion of the fluid elements,

$$\left| \frac{U_f(t) - U_p(t)}{U_f(t)} \right| = \exp\left(-\frac{t}{\tau}\right) \qquad (1)$$

with the relaxation time τ being given by

$$\tau = \frac{d_p^2 \left(\rho_p - \rho_f\right)}{18\mu_f} \qquad (2)$$

Because Eqs. (1) and (2) are derived for a high density ratio, i.e., the density of the particle is much greater than the fluid density, they will provide the worst case scenario estimation of the velocity lag. The light-scattering ability depends on the ratio of the refractive index of the tracer particles to that of water, the particle size and shape, and the light polarization and observation angles. For spherical particles with diameter larger than the incident wavelength, Mie scattering is characterized by the normalized diameter, q, defined as

$$q = \frac{\pi d_p}{\lambda} \qquad (3)$$

An increase in q rapidly increases the ratio of forward-to-backward scatter intensity (Raffel et al., 1998), thus promoting the efficiency of elastic scattering. However, even though the use of short wavelengths with large particles would maximize q, the NIR camera has greater sensitivity at longer wavelengths. In addition, the choice of large tracer particles would undermine their flow-tracking ability by introducing longer relaxation times, as indicated by Eq. (2). Due to these competing considerations, a trade-off is required for the choice of wavelength and particle size.

In the present work, a wavelength of 1350 nm and polystyrene particles of 1.5 µm diameter were found to yield optimal performance. The viscosity of water at 20°C is 1007×10^{-6} N s/m^2, giving a relaxation time $\tau = 6.2$ ns. From Eq. (1), it follows that the relative velocity lag will reduce to 1%

within 28.6 ns. This ensures faithful tracking of the flow, since for the maximum centerline velocity measured in the present work, 1.5 m/s, it will take 40 ms for the fluid element to reach the half-length of the micro-capillary tube, where the measurements are made. In addition, at a wavelength of 1 μm, the refractive indices for polystyrene, water and fused silica are 1.45, 1.33 and 1.55, respectively. The mismatch between these values allows the tracer particles to be clearly distinguished, and the interface between water and fused silica does not cause any serious optical aberration. To further reduce image distortion, the micro-capillary tube is immersed in a layer of water in the experiment.

3

Imaging and analysis

The working principles of standard micro-PIV techniques are described by Santiago et al. (1998) and Meinhart et al. (1999). A number of important components of IR-PIV differ significantly from the standard approach due to the use of infrared instead of visible light, and the lower resolution of the NIR camera (320×256 pixels with 30 μm sensor size) relative to a CCD camera ($> 1024 \times 1024$ pixels with < 10 μm sensor size). Following are details of IR-PIV implementation necessitated by these differences.

3.1

Depth of Field and Measurement Depth

Volume illumination is the only feasible approach since it is impractical to generate and align a light sheet that is only a few micrometers thick as would be required for microdevices. Hence, the depth of field and measurement depth must be carefully determined in order to assess the out-of-plane component.

The depth of field can be calculated (Inoué and Spring, 1997) from

$$\delta z = \frac{n\lambda}{NA^2} + \frac{n\,e}{NA\,M} \qquad (4)$$

where n is the refractive index of the fluid between the objective lens and the test structure, λ is the wavelength of incident light, NA is the numerical aperture of the objective lens, M is the total magnification of the microscope system, and e is the smallest resolvable distance on the image detector, i.e., spacing between pixels. In the present work, $n = 1$ for air, $\lambda \cong 1350$ nm, $M = 20$, and $e = 0$, resulting in a depth of field of $\delta z = 8.44$ μm. The measurement depth describes the distance from the center of the object plane beyond which the particle image intensity will be too low to contribute significantly to the measurement. It is given by (Meinhart et al., 2000)

$$\delta z_m = \frac{3n\lambda}{NA^2} + \frac{2.16 d_p}{\tan(\theta)} + d_p \qquad (5)$$

where $\tan(\theta) \cong NA/n$. With the current optical settings, $\delta z_m = 34.9$ μm.

3.2

Spatial Resolution

Spatial resolution refers to the volume required to make the micro-PIV measurement. The out-of-plane spatial resolution can be determined in terms of measurement depth, which is 34.9 μm in the present work. The in-plane spatial resolution is limited by the effective diameter of particle images

when projected back into the flow field (Meinhart et al., 1999). The actual image recorded on the camera sensor array is the convolution of the diffraction-limited image with the geometric image, which can be estimated as

$$d_e = \sqrt{M^2 d_p{}^2 + d_s{}^2} \qquad (6)$$

where the diameter of the diffraction-limited point spread function in the image plane is

$$d_s = 2.44 M \frac{\lambda}{2NA} \qquad (7)$$

Thus, the effective particle diameter in the current work is $d_e = 87.6$ µm, which implies a particle image resolution of $d_e / M \sim 4.38$ µm in the flow field. As an interrogation window of 32×8 pixels is used, the resulting in-plane spatial resolution is 11.84 µm in the radial direction. The spatial resolution in the streamwise direction does not play an important role in the present work, since the flow is independent of that direction.

3.3

Measurement Uncertainty

Given the pixel size of 30 µm for the NIR camera, the effective particle diameter will be resolved by 3 pixels in the image plane. This is very close to the optimal value recommended for minimizing the overall measurement error (Prasad et al. 1992). The location of the particle image correlation peak can then be determined to within $1/10^{\text{th}}$ the particle image diameter, this translates into a measurement uncertainty, $\delta x \approx d_e / 10M$; in the current work, $\delta x = 321$ nm. Considering the 1 ns resolution of the delay generator and the average particle displacement of 15 µm, the uncertainty associated with velocity measurement is estimated to range from 2% at the center of the tube to 7% in the near-wall region; the higher uncertainty near the walls arises from the much smaller particle displacements.

3.4

Correlation Algorithm

Two statistical algorithms can be used in the digital analysis of PIV recordings according to the way the PIV images are recorded.

For single exposure/double frame PIV, the image pairs are analyzed by means of a cross-correlation algorithm. The two images of the flow field are taken at times t_1 and $t_2 = t_1 + \Delta t$, denoted by $I_1(X)$ and $I_2(X)$. The spatial cross-correlation can be estimated by the convolution integral (Keane and Adrian, 1992)

$$R(s) = \int I_1(X) I_2(X + s) dX \qquad (8)$$

The cross-correlation measures the degree of match between two intensity fields for given spatial shifts, and the particle image displacement can be estimated from the highest value in the correlation plane.

The auto-correlation function for multiple exposure/single frame PIV recordings is calculated in virtually the same manner as for cross-correlation, except that each pair of images analyzed are on the same frame. It should be noted that a large number of such image pairs (as many as 160 images in this work), all recorded on the same frame, are analyzed and the correlation functions are ensemble-averaged in the analysis software. A direct consequence of employing the auto-correlation algorithm is directional ambiguity, and this can be removed through a knowledge of the preferential displacement (*i.e.*, flow) direction. An additional drawback of the auto-correlation approach is the relatively low signal-to-noise ratio (SNR) obtained as compared to cross-correlation. However, as will be discussed further below, auto-correlation is necessary for measuring high-speed velocity fields.

3.5

Timing Sequence

The instantaneous flow field is calculated from consecutive particle images illuminated by the double pulses of the TWIN OPO Nd:YAG laser system. The first laser pulse lasts for 4.9 ns recording the first image field, and after a specified time delay δt, the second laser pulse records the second image field. Depending on the correlation algorithm adopted, double frame/single exposure or single frame/double exposure recordings are acquired. The timing sequence is substantially different based on the correlation approach to be used, as illustrated in Fig. 3 (a) and (b).

If a cross-correlation approach is to be used, the time delay δt between laser pulses must be longer than the straddling time between adjacent video frames, as shown in Fig. 3 (a), so that the image pair may be separated on to two consecutive frames. It is desirable to minimize δt to increase the maximum velocity that can be measured. However, the fixed dead-time regime (≈ 762 µs for the camera used), at the end of each video frame of the NIR camera prohibits an arbitrary reduction in δt. During this time period, any incoming signal will be ignored by the FPA. This hardware constraint limits the maximum measurable velocity to less than 0.3 m/s. At a velocity of 0.3 m/s, only half of the tracer particles can be cross-correlated since the other half will escape the frame on the second image. An auto-correlation approach must be adopted for higher-speed flows. As indicated in Fig. 3 (b), the two lasers are synchronized in one single frame in this approach such that the time interval between the pulses can be arbitrarily varied. Therefore, the auto-correlation approach can work with *any* velocity.

Both cross-correlation and auto-correlation approaches are demonstrated in this work.

4

Results and discussion

Results from the application of the IR-PIV technique to the study of fully developed flows in a circular micro-capillary tube are presented and discussed in the following.

4.1

Fully Developed Flow in a Circular Tube

For laminar flows, the hydrodynamic entry length can be calculated from (Incropera and DeWitt, 1996)

$$\left(\frac{L_{fd}}{D}\right)_{la\min ar} \approx 0.05 \, \text{Re} \qquad (9)$$

with $D = 255$ µm and $Re = 2300$, $L_{fd} \cong 28.75$ mm. The PIV measurements are made at a location half way along the length of the micro-capillary tube in a region well beyond the entry length. The velocity profile for fully developed flow in circular tubes thus provides the theoretical expectation against which to compare the PIV measurements:

$$u(r) = 2u_m\left(1 - \left(\frac{r}{r_0}\right)^2\right) \qquad (10)$$

As shown in Fig. 4, r is the radial position, r_0 is the radius of the tube, u_m is the mean velocity that can be experimentally obtained from the flow rate.

One critical issue in making accurate measurements is the alignment of the test piece with respect to the imaging system. Perfect optical alignment is difficult to achieve, and slight misalignments may cause errors leading to a mismatch with the prediction of Eq. (10). The NIR camera is mounted on a motorized 3-D transverse, due to which the least count for adjustment of the microscope focal plane is 5 μm for this work. Images may thus be acquired in a plane a distance Δr away from the central plane of the tube, as illustrated in Fig. 4. In addition, the optical axis of the microscope may not be strictly perpendicular to that of the tube, introducing an angle θ between the two axes. However, a parabolic velocity profile may still be assumed even in the tilted cross-plane, if Δr and θ are not large. The velocity profile incorporating the effects of axial and angular misalignments, Δr and θ, can be derived from geometrical considerations as:

$$u(r) = 2u_m \left(1 - \left(\frac{\Delta r}{r_0} \right)^2 \right) \left(1 - \frac{r^2}{r_0^2 - (\Delta r)^2} \right) \cos(\theta) \quad (11)$$

With no misalignments, this equation reduces to Eq. (10). The velocity profile from Eq. (11) is used in the following to compare against PIV measurements.

In practice, Δr can be estimated by measuring the nominal tube radius r_{nom} in the recorded images, as

$$\Delta r = \sqrt{r_0^2 - r_{nom}^2} \quad (12)$$

The angle θ cannot be readily measured in the current experiments. However, the influence of θ can be examined in an iterative manner: since θ is very small, an arbitrary value such as 0.1 deg is first assumed in Eq. (11) and the corresponding velocity profile compared to the measured profile at a given flow rate. If the profiles agree, predictions with the same θ-value are used to compare with experiments at all flow rates. By successively incrementing θ by small amounts, the correct value is obtained which matches the predictions for all flow rates. Possible effects of θ on the out-of-plane component of velocity can be neglected, since even at a value of 3 deg, the maximum out-of-plane displacement of tracer particles in the entire field of view would only be 24.5 μm, which is less than the measurement depth of 34.9 μm computed from Eq. (5).

4.2

Low-Speed Measurement (Cross-Correlation)

The cross-correlation approach offers much higher signal-to-noise ratio (SNR) than auto-correlation and therefore, is the desired option for PIV analysis. Due to the hardware constraints on the timing sequence described earlier, it is best suited for very low-speed flows, such as those encountered in bio-medical applications. For such measurements a DynaLite high-intensity illuminator with a dichroic reflector bulb is used as a continuous illumination source instead of the laser light; this source has an adequate IR component for making IR-PIV measurements and can be employed as a quick-and-easy implementation for low-speed measurements. The major benefit in using a continuous source is that the sensors of the NIR camera work much more effectively by capturing more photons during the extended exposure period, i.e. 10 ms for the continuous source vs. 4.9 ns for a laser pulse duration. This helps to distinguish the particles in the measurement plane from those that are out-of-plane. At low flow speeds, the image pair of the same ensemble of tracer particles can still be clearly identified on consecutive images without blurring with long exposure time. A sample image and results of PIV analysis on such images is shown in Fig. 5 (a) to (c) for flow in a micro-capillary tube with $D_h = 255$ μm. The time delay between consecutive frames is 12 ms. An interrogation window of 32×8 pixels and a grid size of 8×4 are used. Adaptive window offsetting methods – central difference interrogation (CDI) and continuous window shifting (CWS) – are employed with an FFT-based correlation algorithm to improve the reliability and accuracy of the PIV measurement. In the theoretical velocity profiles shown in the figures, the mean velocity is obtained from the flow rate measurement, and the centerline position of micro-capillary tube is determined from the maximum velocity of experimental measurement. The parabolic nature of the measured velocity profile is clearly discernible in Fig. 5 (b), with a maximum velocity of 500 μm/s. Using this maximum velocity u_{max} ($= 2u_m$) and the diameter of micro-capillary tube r_0, the expected velocity profile from Eq. (11) is plotted in Fig. 5 (c), and seen to agree well in terms of profile shape with the measurements.

4.3

Moderate to High-Speed Measurement (Auto-Correlation)

Measurements for higher flow rates are performed using auto-correlation, for a variety of flow rates. A sample image (at Re = 126) is shown in Fig. 6. As compared to Fig. 5 (a), the SNR is seen to be considerably lower due to the background noise caused by the out-of-plane particles. However, the double exposures of the identical particles can still be distinguished. It can also be seen that the particle displacements are largest at the center and decrease towards the wall. As pointed out earlier, the frame straddling time can be flexibly adjusted so that the auto-correlation approach applies to much higher velocities, at which the cross-correlation approach fails.

Results of the PIV analysis are shown at three different flow rates in Fig. 7 (a) to (c). The time delays for the three cases are 58, 33 and 26 µs, respectively. The theoretical prediction is calculated using the experimentally measured mean flow rate. The excellent agreement for all three cases demonstrates the efficacy of the IR-PIV technique. Due to the decrease in SNR and the auto-correlation processing, velocities could not be obtained near the walls. However, a majority of the velocity profile is correctly captured by PIV measurement to within ±5% of the theoretical prediction. Better measurements can be acquired in the future work by using two different time delays for given flow rate. The shorter δt will yield accurate measurements for the center of the tube, while the longer δt will allow accurate measurements closer to the wall. The highest velocity measured in the current work was 1.5 m/s with a pressure head of 0.4 MPa. While significantly higher velocities can be measured with this technique by adjusting the time delay, the current setup has limitations on the sealing of the micro-capillary tube beyond these pressure heads.

5

Conclusions

A non-intrusive diagnostic technique, infrared micro-particle image velocimetry (IR-PIV), has been presented for measuring flow fields within MEMS devices with micron-scale resolution. The working principles and important technical aspects of the technique, such as illumination, choice of tracer particle, timing sequence, imaging technique and the micro-PIV analysis algorithm, etc., are discussed. The utility of the technique is demonstrated through experiments on laminar flow in micro-capillary tubes.

Experiments have been conducted in the present paper both for low and moderate-to-high speed flows. In ongoing work, the potential of this novel technique will be further explored by extending it to measurements in microchannel heat sinks. In addition, since very fine tracer particles (~ 1 µm) are used in this work, Brownian motion of the particles is measurable and often intentionally reduced to avoid errors in velocity measurement. However, there is evidence (Olsen and Adrian, 2000; Hohreiter, et al., 2001) that the broadening of the cross-correlation peak caused by Brownian motion may be used correlated to the temperature of the flow. Further exploration of this temperature measurement approach may allow the present IR-PIV technique to be extended for obtaining simultaneous velocity and temperature measurements in silicon-based micro-devices.

Acknowledgements

References

Breuer K; Bird JC; Han G; Westin KJ (2001) Infrared Diagnostics for the Measurement of Fluid and Solid Motion in Micromachined Devices. ASME International Mechanical Engineering Congress and Exposition, New York, NY, Nov. 11-16

Chung J; Grigoropoulos CP; Greif R (2003) Infrared Thermal Velocimetry in MEMS-Based Fluidic Devices. J MEMS 12: 365-372

Garimella SV; Sobhan CB (2002) Transport in Microchannels – A Critical Review. Annual Review of Heat Transfer 13

Hohreiter V; Wereley ST; Chung JN; Olsen MG (2001) Cross-correlation Analysis for Temperature Measurement. Proceedings of 4th International Symposium on Particle Image Velocimetry, #1145, Göttingen, Germany, September 17-19

Incropera FP; DeWitt DP (1996) Fundamentals of Heat and Mass Transfer. John Wiley & Sons, Inc., N. Y.

Inoué S;Spring KR (1997) Video Microscopy. Oxford, Plenum Press

Keane RD; Adrian RJ (1992) Theory of Cross-correlation Analysis of PIV Images. Applied Science Research 49: 1-17

Lanzillotto AM; Leu TS; Amabile M; Wildes R; Dunsmuit J (1996) An Investigation of Microstructre and Microdynamics of Fluid Flows in MEMS. Proc. ASME Aerospace Division AD-52, pp.789-795.

Liu D; Garimella SV (2004) Investigation of Liquid Flow in Microchannels. J Therm. Heat Trans. 18: 65-72

Melling A (1997) Tracer Particles and Seeding for Particle Image Velocimetry. Meas. Sci. Tech. 8: 1406-1416

Meinhart CD; Prasad AK; Adrian RJ (1993) A Parallel Digital Processor for Particle Image Velocimetry. Meas. Sci. Tech. 4: 619-626.

Meinhart CD; Wereley ST; Santiago JG (1999) PIV Measurement of a Microchannel Flow. Exp Fluids 27: 414-419

Meinhart CD; Wereley ST; Gary MHB (2000) Volume Illumination for Two-dimensional Particle Image Velocimetry. Meas. Sci. Tech. 11: 809-814

Olsen MG; Adrian, RJ (2000) Brownian Motion and Correlation in Particle Image Velocimety. Optics and Laser Technology 32: 621-627

Prasad AK; Adrian RJ; Landreth CC; Offutt PW (1992) Effect of Resolution on the Speed and Accuracy of Particle Image Velocimetry Interrogation. Exp Fluids 13: 105-116

Raffel M;Willert C; Kompenhans J (1998), Particle Image Velocimetry: A Practical Guide, Springer

Santiago JG; Wereley ST; Meinhart CD; Beebe DJ; Adrian RJ (1998) A Particle Image Velocimetry System for Microfluidics. Exp Fluids 25: 316-319.

Wu D; Chen A; Johnson CS (1995) Flow Imaging by Means of 1D Pulsed-Field-Gradient NMR with Application to Electroosmotoc Flow. J Magn. Reson. Ser. A. 115: 123-126

www.thermo.com/com/cda/resources/resources_detail/1,2166,10278,00.html
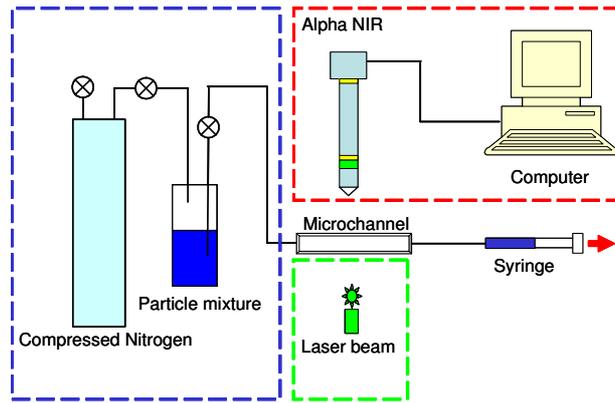
List of figure captions

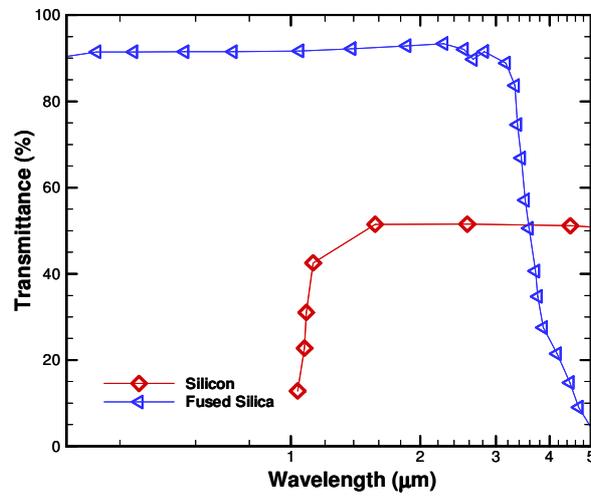Fig. 1. Schematic of experimental apparatus.

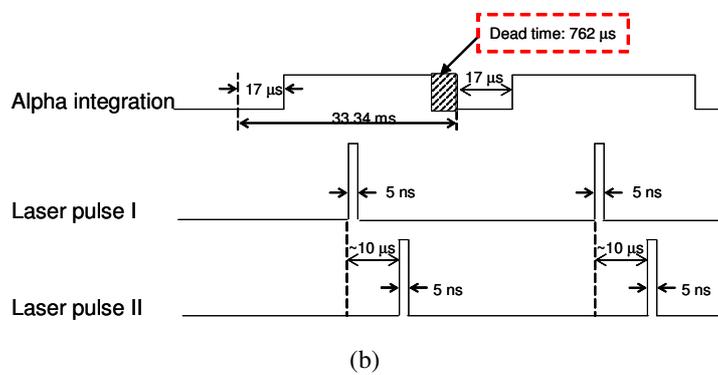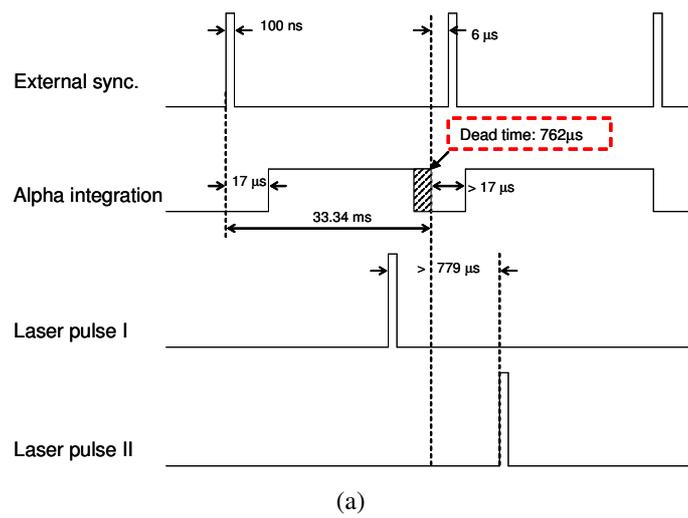Fig. 2. Transmittance curves for silicon and fused silica.

Fig. 3. Timing sequences: (a) Cross-correlation for low-speed measurement, and (b) Auto-correlation for moderate to high-speed measurement.
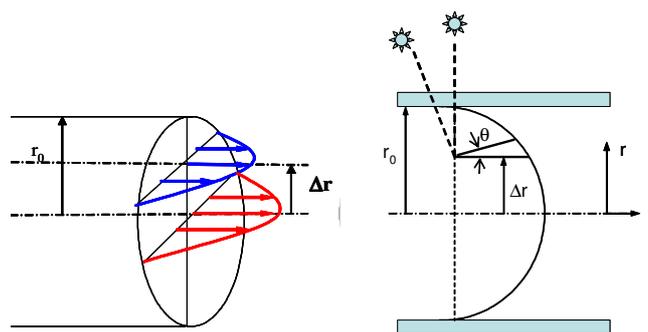
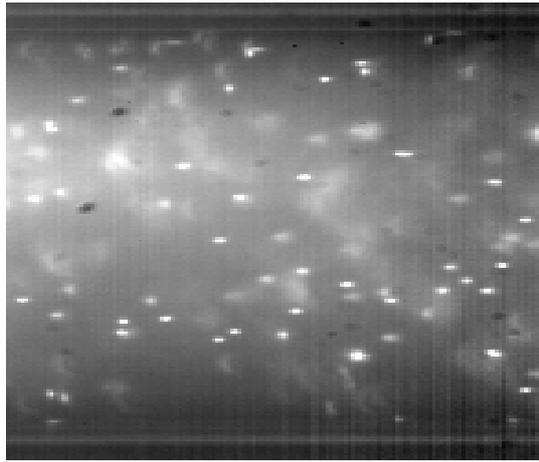Fig. 4. Velocity profile for misaligned optics.

Fig. 5. IR-PIV results for very low-speed flow: (a) sample image, (b) velocity vectors, and (c) comparison of the measurements with the theoretical profile.

Fig. 6. PIV image at a higher flow rate (Re = 126).

Fig. 7. IR-PIV results for moderate-to-high speed flows: (a) $u_m = 0.35$ m/s (Re = 88), (b) $u_m = 0.50$ m/s (Re = 126), and (c) $u_m = 0.77$ m/s (Re = 195).

Fig. 1. Schematic of experimental apparatus.

Fig. 2. Transmittance curves for silicon and fused silica.

(a)

(b)

Fig. 3. Timing sequences: (a) Cross-correlation for low-speed measurement, and (b) Auto-correlation for moderate to high-speed measurement.
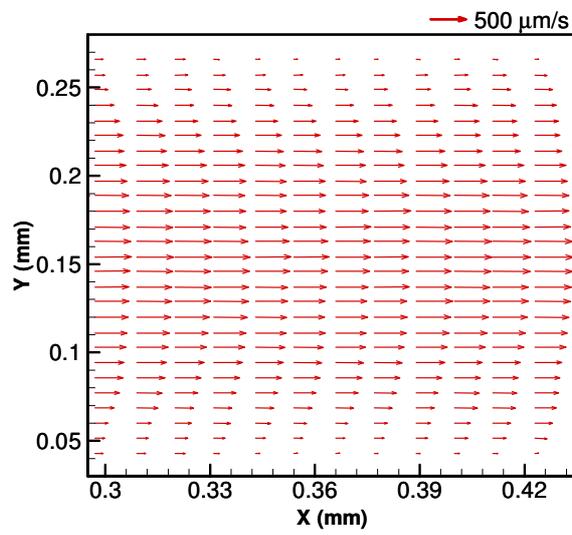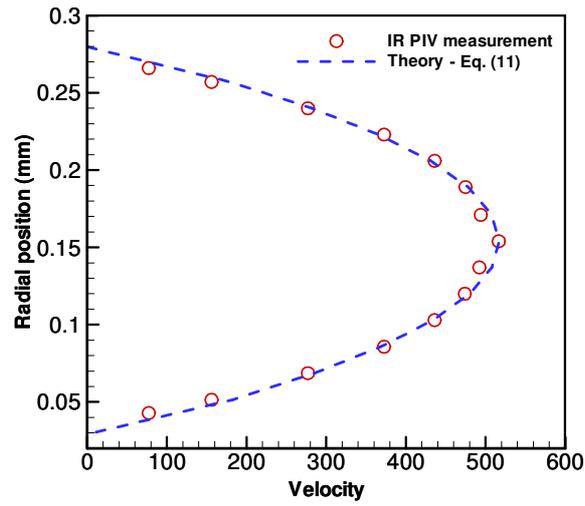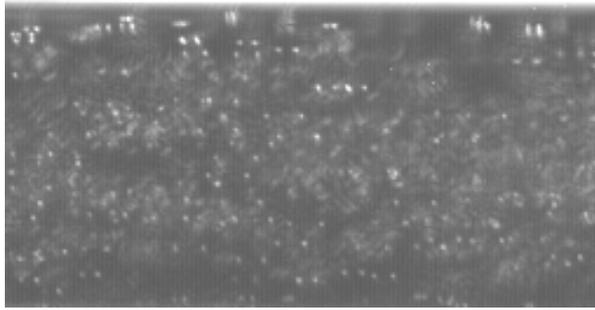

Fig. 4. Velocity profile for misaligned optics.

(a)

(b)

(c)

Fig. 5. IR-PIV results for very low-speed flow: (a) sample image, (b) velocity vectors, and (c) comparison of the measurements with the theoretical profile.
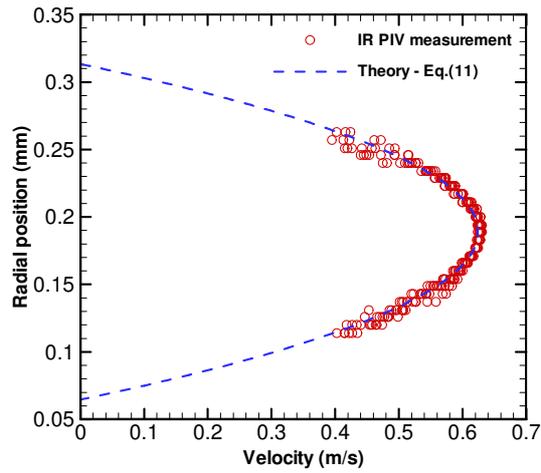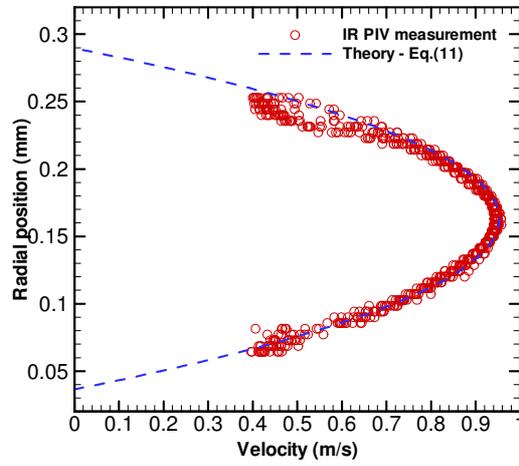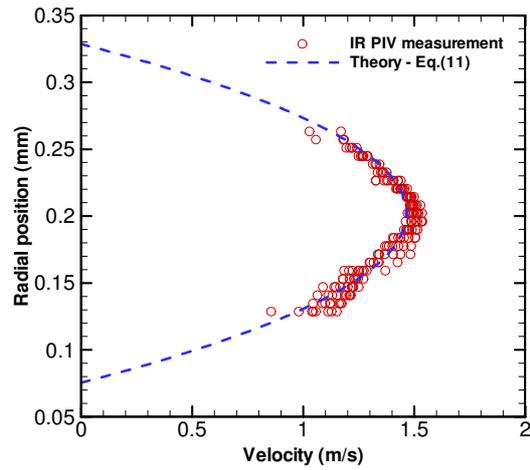
Fig. 6. PIV image at a higher flow rate (Re = 126).

(a)

(b)

(c)

Fig. 7. IR-PIV results for moderate-to-high speed flows: (a) $u_m = 0.35$ m/s (Re = 88), (b) $u_m = 0.50$ m/s (Re = 126), and (c) $u_m = 0.77$ m/s (Re = 195).